ADVANCED MATERIALS INTERFACES
Open Access
www.advmatinterfaces.de

Turning Plastic Waste Immiscibility into an Advantage: Efficiency Improvement of PVDF-Based Energy Harvesters Using Post-Consumer Thermoplastics

Petr Slobodian, Berenika Hausnerova, Pavel Riha, Vladimir Pata, Robert Olejnik, and Jiri Matyas*

The immiscibility of plastic waste, which is often a limiting factor in traditional recycling processes, is considered in this study as a key feature for functional material design. Polyvinylidene fluoride (PVDF), renowned for its exceptional triboelectric and piezoelectric properties, is combined with post-consumer thermoplastic waste from the packaging industry to create a novel, sustainable energy-harvesting solution. Immiscible compounds of wasted high-density polyethylene, polypropylene, polystyrene, and polyethylene terephthalate form physical mixtures of domains of individual polymers within the melt, which enhance mechano-electric conversion when paired with PVDF to achieve a remarkable output voltage of 800 V, with short-circuit current and charge densities reaching 260 μAcm^{-2} and 710 nCm^{-2}, respectively, surpassing traditional PVDF-nanoparticle composites. This method not only reduces reliance on costly nanomaterials but also demonstrates the potential of repurposed plastic waste for energy applications. The design of the sensors is examined to distinguish the contribution of piezo- and tribo-electrifications. Examples of low-cost sustainable sensors constructed from PVDF and thermoplastic waste films demonstrate efficient energy conversion and sensitivity to mechanical stimuli and highlight the potential of repurposing immiscible plastic waste not only as a solution to pollution but also as a contributor to green energy technologies.

1. Introduction

Polyvinylidene fluoride (PVDF) is the most frequently studied polymer because of its favorable triboelectric and piezoelectric efficiencies. It is chemically stable, lightweight, and highly flexible. Its exceptional piezoelectric properties are significantly enhanced in the β-phase and can be further increased by incorporating fillers. Nanogenerators utilizing PVDF have demonstrated substantial potential for converting mechanical energy into electrical energy, which is suitable for powering small electronic devices and sensors. PVDF is used in hybrid devices that combine triboelectric and piezoelectric mechanisms, where liquid-solid interactions play a role in energy harvesting.[1]

Recent advancements have focused on enhancing the performance of PVDF-based nanogenerators via various modifications. Incorporating carbon-based nanomaterials, such as graphene and carbon nanotubes, into PVDF matrices has been shown to improve their piezoelectric response, thereby increasing their energy conversion efficiency.[2] The development of flexible PVDF nanocomposites embedded with magnetic nanoparticles, such as cobalt ferrite ($CoFe_2O_4$), has led to the development of nanogenerators capable of harvesting energy from both mechanical and magnetic sources. These flexible devices exhibit enhanced power efficiency, highlighting their potential for integration into wearable electronics and other applications that require adaptable energy-harvesting solutions.[3] Further studies demonstrated that PVDF-based piezoelectric and

P. Slobodian, P. Riha
Department of Physics and Materials Engineering
Faculty of Technology
Tomas Bata University in Zlín
Vavreckova 5669, Zlín 760 01, Czech Republic

P. Slobodian, B. Hausnerova, R. Olejnik, J. Matyas
Centre of Polymer Systems
University Institute
Tomas Bata University
Trida T. Bati 5678, Zlin 76001, Czech Republic
E-mail: hausnerova@utb.cz

B. Hausnerova, P. Riha, V. Pata
Department of Production Engineering
Faculty of Technology
Tomas Bata University in Zlin
Vavreckova 5669, Zlín 760 01, Czech Republic

The ORCID identification number(s) for the author(s) of this article can be found under https://doi.org/10.1002/admi.202500070

DOI: 10.1002/admi.202500070

triboelectric systems could be used in diverse biomedical and sustainable energy applications.[4–6] For instance, Panda et al.[4] explored piezoelectric energy-harvesting systems tailored for biomedical applications, showcasing the potential of PVDF composites in practical scenarios. Niranjana et al.[5] reported the enhancement of triboelectric performance by electrospinning PVDF-based hybrid fibers, emphasizing the importance of structural modifications to achieve improved efficiency.

Venkatesan et al.[6] developed flexible triboelectric sensors using cobalt ferrite-embedded PVDF nanocomposites for healthcare applications, underlining the importance of material choices and fabrication techniques.

Output voltage values of PVDF can be further enhanced by its combination with other polymers as shown for triboelectric nanogenerator (TENG) made of PVDF combined with polyamide 6 resulting in 384 V and 26.4 μC m^{-2},[7] or recently reported biaxially-oriented polyethylene terephthalate films paired with PVDF showing superb 624 V open-circuit output.[8] However, the harvesting efficiency of PVDF is mostly enhanced by its combination with rather expensive materials, as shown by Kujawa et al.[2] in a comprehensive overview of the current and future applications of PVDF-carbon nanomaterials in energy and sensing.

The aim of this study is different - to develop cost-effective and sustainable materials for sensing applications exploring the potential of immiscible thermoplastic waste from post-consumer sources such as food packaging. The vast majority of such mixed thermoplastic waste still ends up landfilled,[9] and mechanical-electric energy conversion can contribute to its new efficient functionality because mechanical energy harvesting is a green technology with great potential for applications in self-powered portable electronics, wireless sensing, implanted devices, and security systems.[10–12]

There have already been some attempts in this research direction; however, they mainly use expensive advanced techniques to transform plastic waste into new functional materials. For example, expanded polystyrene (PS) waste was dissolved to obtain fibers by electrospinning, which were then fabricated into laminates.[13] A TENG intricately fabricated from recycled graphite and PET bottles achieved an open-circuit voltage of 84 V and short-circuit current of 101 μA, with a maximum power density of 26 μW cm^{-2}.[14] In addition, combinations of polyamide, polyvinylidene chloride, and polyethylene (PE) films yield promising voltage outputs.[15] Creative reuse of medical waste has led to innovations such as TENGs from saline bottles, delivering 8.78 W/m^2, and powering 420 LEDs in vertical contact separation mode.[16] Similarly, TENGs utilizing polypropylene (PP) face masks and Mylar (PET) sheets achieved 200 V and 0.29 mA m^{-2} current density, albeit requiring UV-C disinfection.[17] Indium tin oxide-coated PET paired with PET resulted in the output voltage and current of 224 V, and 80 μA, respectively.[18] Laboratory waste materials such as aluminum, cotton, and nitrile gloves have been used in TENGs to power exercise counters and safety devices.[19] Khandelwal et al.[20] fabricated TENGs using PE and PP waste as the negative triboelectric layer and kitchen sponges as the positive layer, achieving an output of 44 V and 289 nA. Other waste materials (bio-waste, medical non-plastic waste, etc.) serving as TENG have been recently summarized in.[21]

In the present work, no time-demanding or expensive technique is needed to redesign thermoplastic waste. The selection of waste materials reflects the real-world composition of post-consumer plastic waste,[22] which typically originates from common applications such as food packaging, bottles, and trays. Polyvinylidene fluoride is paired with essentially immiscible waste compounds containing high-density polyethylene, polypropylene, polystyrene, and polyethylene terephthalate bottles and food trays from trash bins and subjected to coupled tribo-piezoelectric electrification with the aim of finding synergy to obtain remarkable values of the generated voltage.

2. Experimental Section

The PVDF fiber membrane was prepared by electrospinning PVDF powder dissolved in dimethylformamide. The electrospun fibers were stretched and dried on a polypropylene substrate, as described in a previous study.[23] The PVDF fibrous membrane has a homogeneous structure formed by individual submicron-sized PVDF fibers with fiber diameters of ≈0.05–0.3 μm, **Figure 1**; NOVA NanoSEM 450, FEI Co., Hillsboro, OR, USA). The compounds were prepared from commodity waste as soft drink bottles, dishwashing liquid bottles, meat packaging trays, and cheese trays, marked with numbers according to the plastic classification codes recommended by the Society of the Plastics Industry as 1 - PET, 2 - HDPE, 5 – PP and 6 – PS, respectively. The identification was confirmed by infrared spectroscopy (Nicolet iS 5 FTIR Spectrometer, Thermo Fisher Scientific, Waltham, MA, USA). The compounds were prepared in a molten state using a mixer (MB 50 Brabender GmbH & Co. KG, Duisburg, Germany) at 265 °C for 10 min at 50 rpm, with the following compositions in wt.%: 25PS/25PET/25HDPE/25PP, 60PET/40PS-HDPE-PP (presented equally), and 60PS/40PET-HDPE-PP (presented equally). The prepared compounds were immiscible and were formed by domains of individual polymers (see Figure 1).

A 3D scanner (Zygo NewView 8000, AMETEK, Inc., Middlefield, Connecticut, United States) was used for surface scanning. The profilometer is a powerful interferometric system with Coherence Scanning Interferometry (CSI) technology, which combines Vertical Scanning Interferometry (VSI) and Phase Shifting Interferometry (PSI). The surface roughness parameters were evaluated according to the ISO 21920-2 standard.

The relevant physical properties of PVDF, thermoplastic waste, and their compounds are summarized in **Table 1**. The melting temperatures (T_m) and glass temperature (T_g) of PS were obtained as the maximum peak temperatures determined by differential scanning calorimetry (DSC 1, Perkin Elmer, Waltham, MA, USA). The mechanical properties, in terms of tensile strength (s), were determined using a tensile test machine (M350-5CT, Tensometric, Manchester, UK) at a velocity of 10 mm per min. The dielectric constant (e) and dielectric loss (tan d) were measured using a broadband dielectric/impedance analyzer (Novocontrol Technologies GmbH & Co. KG, Montabaur, Germany). Samples of a particular thickness were placed between two gold-plated electrodes with a diameter of 20 mm and tested in the frequency spectrum from 1 Hz to 1 MHz at room temperature. Relative permittivity was measured using a broadband dielectric/impedance analyzer (Novocontrol Technologies GmbH & Co. KG, Montabaur, Germany).

The test films for the conversion were prepared from the compounds by compression molding at 200 °C. The thickness of

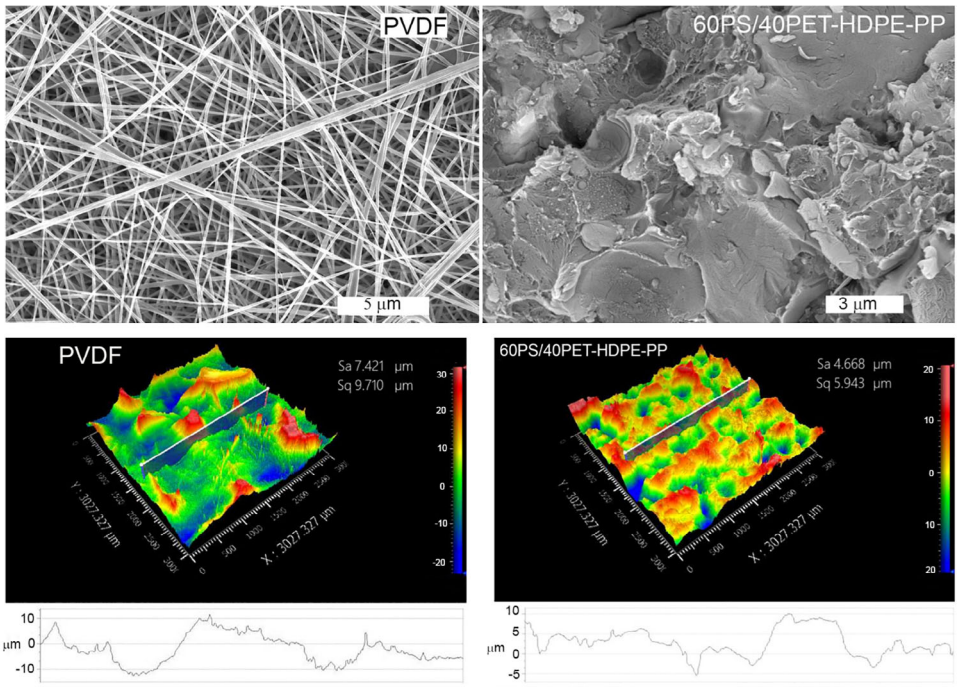

Figure 1. Scanning electron micrographs (NOVA NanoSEM 450, FEI Co., Hillsboro, OR, USA) and surface topography/cross-sectional profiles (Zygo NewView 8000, AMETEK, Inc., Middlefield, CT, USA) of PVDF membrane and immiscible thermoplastic waste compound (60PS/40PET-HDPE-PP).

the thermoplastic waste samples was kept uniform at (0.13 ± 0.01) mm and the PVDF layer was 0.02 mm thick. Electricity generation was carried out using an experimental setup consisting of PMMA plates with copper electrodes equipped with four metal guides and springs to allow their movement upon touching. Cuprexit was used as an electrode (Cu foil on a glass epoxy substrate; the thicknesses of the Cu foil and the substrate were 35 and 200 µm, respectively). A waste sample was attached to the first electrode, whereas a PVDF sample was attached to the second electrode as a triboelectric pair material. To measure the applied maximum force, a strain gauge L6D-C3-40 kg (Zemic Europe B.V., Etten-Leur, Netherlands) was used. In addition, the velocity of contact was measured to be 0.85 m/s. A DSO-Digital Storage Oscilloscope (Infinivision 1000 x-series, 4ch, 100 MHz, DSOX1204A, Keysight, Santa Rosa, CA, USA) was used to measure the generated output voltage. The charge generated in one cycle was measured using a Vernier CRG-BTA charge sensor (Vernier, Beaverton, OR, USA) connected to the LabQuest interface system (Edufor s.r.o., Prague, Czech Republic).

Table 1. Physical properties of the tested materials.

Parameter	T_m/T_g [°C]	σ [MPa]	ϵ [–]	tan δ [–]
PVDF	177.5	14.7 ± 2.1	6.49	0.214
25PS/25PET/25HDPE/25PP	–	3.0 ± 0.8	2.93	0.046
60PET/40HDPE-PS-PP	–	8.5 ± 2.5	2.48	0.047
60PS/40HDPE-PET-PP	–	2.5 ± 0.8	2.53	0.011
PET	250.5	78.6 ± 2.6	3.19	0.012
PS	104.1	19.3 ± 0.7	4.80	0.145
HDPE	133.1	19.1 ± 1.3	2.97	0.041
PP	160.4	26.3 ± 1.9	2.40	0.017

3. Results and Discussion

Piezoelectric and triboelectric electrification processes can be combined for the same type of mechanical energy conversion with an integrated electric energy output. The nanogenerator is schematically illustrated in **Figure 2**, where compression-molded films are subjected to contact-induced coupled electrification of the thermoplastic waste compounds in the tribological pair with a PVDF fiber membrane contact layer on the anode, which were pressed 6 mm against each other cyclically at a velocity of ≈0.85 m s^{-1} and a maximum pressure between the contacting polymers 270 kPa.

The nanogenerator cannot distinguish the individual contributions of the piezoelectric and triboelectric effects to total electrification. However, the electrodes of the oscilloscope detected a positive output voltage at which induced triboelectricity prevailed. As shown in **Figure 3**, the nanogenerators took advantage of the strong triboelectric effect of the thermoplastic waste combined with PVDF to achieve high output voltages: from 120 V for 25PS/25PET/25HDPE/25PP, 200 V for 60PS/40PET-HDPE-PP, to considerably high 800 V for 60PET/40PS-HDPE-PP. The corresponding short-circuit current and charge densities for this composition of thermoplastic waste (60PET/40PS-HDPE-PP) paired with PVDF were 260 ± 23 mAcm^{-2} and 710 ± 24 nCm^{-2}, respectively.

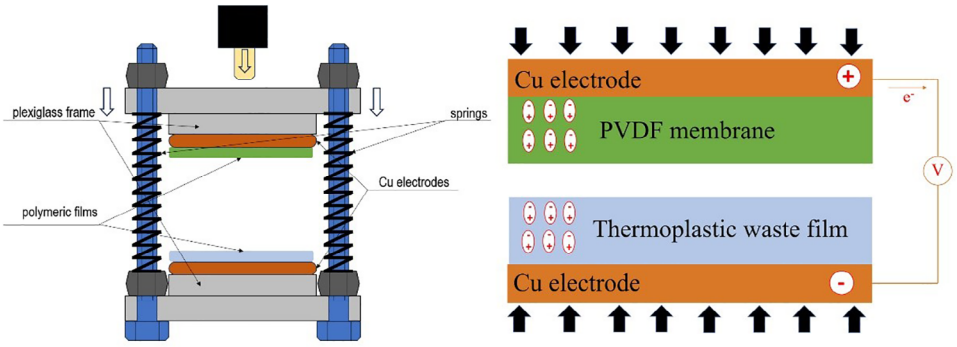

Figure 2. A scheme of coupled triboelectric-piezoelectric nanogenerator.

A series of around 25 cycles were recorded to evaluate the repeatability and consistent performance of the nanogenerator for the most efficient triboelectric pair of PVDF film and 60PET/40PS-HDPE-PP thermoplastic waste blend to ensure high reproducibility and structure stability of the tested materials, **Figure 4**.

Further, the considerable value of the output voltage (800 V) was compared with other recently reported PVDF-based nanogenerators, **Table 2**. As can be seen, only PVDF combined with high performance (high relative permittivity and piezoelectricity) and high-cost $BaTiO_3$ nanoparticles achieved higher (900 V, at 5 Hz, 180 N contact force, 100 mm spacer) output voltage. Post-consumer thermoplastic waste thus provides more sustainable, low-cost (both materials and fabrication) and competitive performance.

The differences in triboelectric performance of the selected waste compositions generally arise from the variation in polymer surface chemistry, roughness, and charge affinity. The roughness of the polymer waste has not been altered, the used plastic packaging materials were used as received. The results are in accordance with the triboelectric series shown in **Figure 5**, where the materials are ranked based on their ability to generate positive or negative charges when in contact with PVDF. The relative permittivity (depicted in Table 1) also affects the output voltages obtained.[34–37] PVDF is a high permittivity material (6.49), while the relatively high permittivity of PS (4.80) and PET (3.19) are compensated with polyolefins. Thus, the relative permittivity of the blends does not exceed the value of 3.

Concerning surface chemistry, FTIR spectra of pure polymers and their blends revealed mutual polymer interactions through peak shifts, intensity reductions, and even peak disappearances, **Figure 6**. The key spectral changes, such as the disappearance of the 698 cm^{-1} and 3021 cm^{-1} peaks of PS in PET-rich blend, the shift of HDPE stretching vibrations (2917 and 2848 cm^{-1}) in PET60PET/40PS-HDPE-PP, and modifications in the PP methyl bending peak (1376 cm^{-1}), indicate significant molecular interactions affecting the vibrational environment of each polymer. These results provide strong evidence of intermolecular interactions, suggesting that waste composition influences molecular packing and structural arrangement. The spectral shifts further indicate that PET and PS interact strongly, likely via π-π stacking and dipolar interactions, altering the molecular environments of each polymer, while PS significantly impacts HDPE structural organization, potentially affecting its crystallinity. Minor spectral shifts in PP suggest molecular packing effects.

The AC voltage generated by the mechanoelectrical conversion of the nanogenerator was rectified into a DC signal using Schottky diodes (diode-opening voltage of 1.5 V) connected to either full- or half-bridge rectifiers. The resulting DC charge was stored in a mica capacitor (4 nF capacitance). This harvesting principle

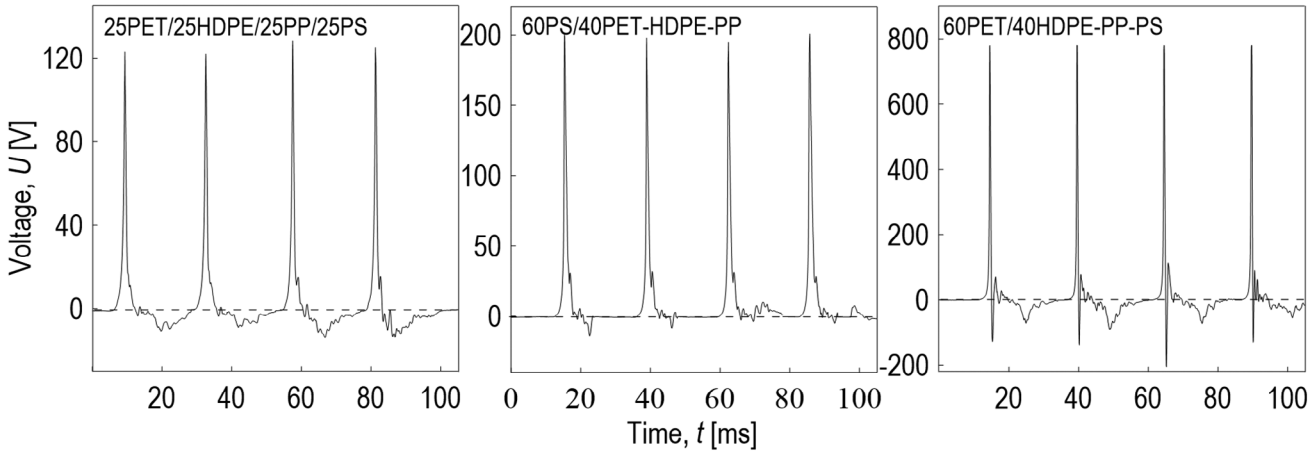

Figure 3. The output voltage of the nanogenerators made of PVDF film and blends of thermoplastic wastes 25PS/25PET/25HDPE/25PP, 60PS/40PET-HDPE-PP, and 60PET/40PS-HDPE-PP.

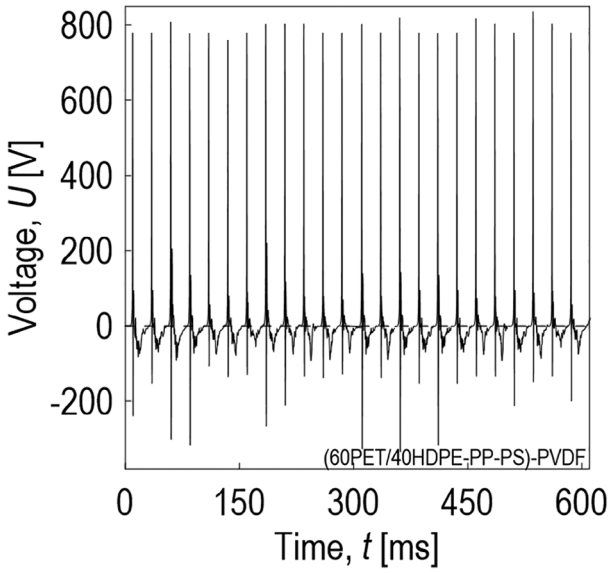

Figure 4. The stability test of the nanogenerator made of PVDF film and 60PET/40PS-HDPE-PP thermoplastic waste.

is illustrated by the diagrams in **Figure 7**. After charging the capacitor for 5, 10, 20, and 40 charging cycles, once by a full-bridge or half-bridge, the charged capacitor was short-circuited. A triboelectric pair combining 60PET/40PS-HDPE-PP with PVDF was used. As a practical demonstration of the efficient transformation of mechanical energy to electricity, it is possible to obtain usable electrical energy in this way. Several LED diodes connected in series - five red LEDs for the full-bridge and seven green LEDs for the half-bridge rectifier–were turned on. The duration of lighting was ≈10 ms. The subsequent discharge of the stored charge by the short-circuit method provided time-dependent discharge behavior, as depicted in Figure 7. The charge harvested as the resulting discharge voltage was measured using an oscilloscope. After the short circuit, the voltage exhibited a significant peak before decreasing exponentially to zero with time. The discharge times for all measurements shown in Figure 7 were 250 ms after the short circuit and were independent of the initial charge level of the capacitor, indicating that they were not affected by the number of cycles, unlike the peak size, which increased with the number of stored cycles.

Table 2. Performance of PVDF-based nanogenerators - output voltage *U*, current *I* and power density *P*.

Material	*U* [V]	*I* [μA]	*P* [W m^{-2}]	Method
P(VDF-TrFE)/BNNTs[24]	22	–	0.113	contact-separation
PVDF/$BiCl_3$/ZnO[25]	12	0.08	6.4	contact-separation
PVDF/$CaTiO_3$[26]	20	0.25	0.0019	contact-separation
PVDF/PDMS/MoS_2[27]	35	20.8	2.2	contact-separation
PVDF/$BaTiO_3$[28]	50	312	0.00407	bending-releasing
PVDF/$CsPbBr_3$[29]	103	170	0.14	pressing
PVDF/Si-HBP-G2[5]	130	3.5	0.225	contact-separation
PVDF/PS[30]	166	11.1	0.662*	contact-separation
PVDF/TrFE/MXene[31]	270	140	4.02	contact-separation
PVDF/Zeolitic Imidazol[32]	395	95	3.1	contact-separation
PVDF/PET[8]	624	61	-	contact-separation
PVDF/Siloxane[33]	646	276	13.25	contact-separation
PVDF-BaTiO3/PA6[7]	900	10	34.4	contact-separation

Both types of rectifiers, full- and half-bridges, were tested to confirm the findings of Ghaffarinejad et al.[38] that the half-bridge is a more efficient variant for collecting the electric charge generated from TENG sources than the full-bridge. However, as shown in Figure 7, the maximum voltage rectified by the half-bridge after 40 cycles was 220 V, whereas it reached ≈430 V when the full bridge was used. Although more complex and expensive, the full-bridge rectifier directs both sides of the voltage wave and can store a larger generated charge per harvesting cycle.

This triboelectrification principle can be successfully used for the construction of self-powered sensors for the detection of deformation or mechanical stress. The connected challenges are related to the design and construction of functional and easily applicable sensors when two layers of a triboelectric pair move against each other. The simplest solution is that the individual parts of the sensor are already layered prior to the application of a mechanical stimulus, and thus the dielectrics would not move macroscopically relative to each other. The layered structure assembled in this manner was then simply placed on the examined object.

The tests show that this arrangement, despite the fact that the layers of the triboelectric pair do not move macroscopically to each other, is capable of detecting the mechanical stimulus of a pressure pulse. This type of sensor is schematically illustrated in **Figure 8**. It consists of two copper electrodes between which a polymer dielectric in the form of a film is placed and fixed with electrically conductive adhesive layers (ECAL), which are a part of the used Cu tape. This set-up was then placed on the solid base and covered with a steel plate on the top to ensure the homogeneous distribution of the pressure pulses exerted by the DC 12V linear solenoid. The steel plate also served as mechanical protection. The steel plate pressed the individual layers together, generating an assembly pressure of 0.2 kPa on the sample area of (25 × 25) mm. The mechano-electrical responses to the solenoid-induced pressure pulse of the PVDF film (Figure 8a) and the film containing 60PET/40HDPE-PS-PP (Figure 8b) were tested.

The dielectric is mechanically polarized, and the charge of the polarization of the dielectric must be compensated by the charge that is transferred from the upper Cu electrode by an external electrical circuit, which represents a positive response to the pressure pulse measured by an oscilloscope. In addition to attaining the desired adhesion, the ECAL is in a rubbery state; thus, the protrusions of the polymer film resulting from their surface roughness are pushed into it, and mutual movement is further prevented when the solenoid pressure is applied. The arithmetic mean of the surface height was Sa = 7.421 μm, the root mean square roughness was Sq = 9.710 μm, and the peak-to-valley height was Sz = 54.904 μm for PVDF. The surfaces of the polymeric films were finer, the 60PET/40HDPE-PS-PP film had Sa = 4.668 μm, Sq = 5.943 μm, and Sz = 39.832 μm. The roughness parameters of the Cu electrode showed a very fine surface with Sa = 0.621 μm, Sq = 0.731 μm, and Sz = 4.369 μm.

The ECAL seems to significantly suppress possible triboelectrification at the interface of the polymeric film and the Cu

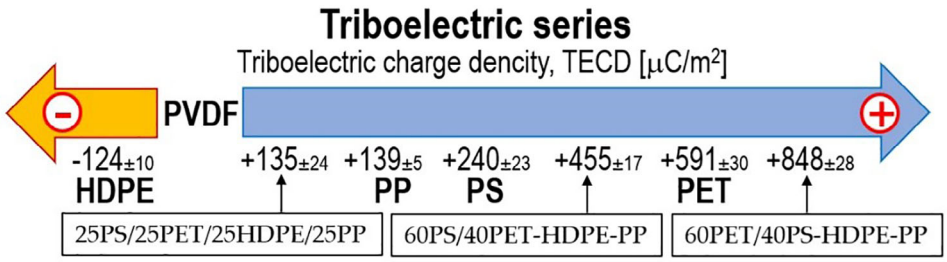

Figure 5. Triboelectric series derived from triboelectrification measurements displaying relative triboelectric polarity of tested materials in respect to PVDF.

electrode. The maximum output voltage for 60PET/40HDPE-PS-PP reached the value of 0.8 V, and for PVDF it raised to 5 V. In the case of 60PET/40HDPE-PS-PP, piezoelectricity is attributed to the polarization of inorganic particles added by the manufacturers during packaging processing to reduce friction, unwanted electric charges, improve mechanical properties, or as a pigment.[39] Energy-dispersive X-ray spectroscopy analysis confirmed the presence of SiO_2 in the PET bottle, $CaCO_3$ in PP, TiO_2 in the PS tray, and traces of it also in the HDPE dish wash liquid bottle. Elements such as Cl, Na, K, and traces of S were attributed to surfactant residues.

In this experiment, ECAL was used to fix the polymer film on the surface of the electrodes to suppress possible triboelectric effects at this interface. Although the two materials already adhere to each other before applying the pressure stimulus, owing to the roughness of the surfaces, a triboelectric effect can occur at the interface. **Figure 9** shows the experimental arrangement with one Cu electrode glued to the polymeric film by the ECAL, and the other electrode pressed towards the polymeric film by the sensor assembly pressure of 0.2 kPa. The mechano-electric response of the 60PET/40HDPE-PS-PP polymeric film reached significantly higher values than when testing the same material fixed to both electrodes owing to triboelectrification at the Cu electrodes and 60PET/40HDPE-PS-PP film interface. Compared to Figure 8, an increase from 0.8 V to +3 V to −6 V can be seen upon a firm fixation on the Cu electrode on one side only (Figure 9).

It has been demonstrated that polarization at the interface of the copper electrode and the tested polymer film can significantly contribute to the total mechano-electrical response. Because the materials have a certain roughness, when a mechanical stimulus is applied, electrification also occurs at the interface due to triboelectrification.

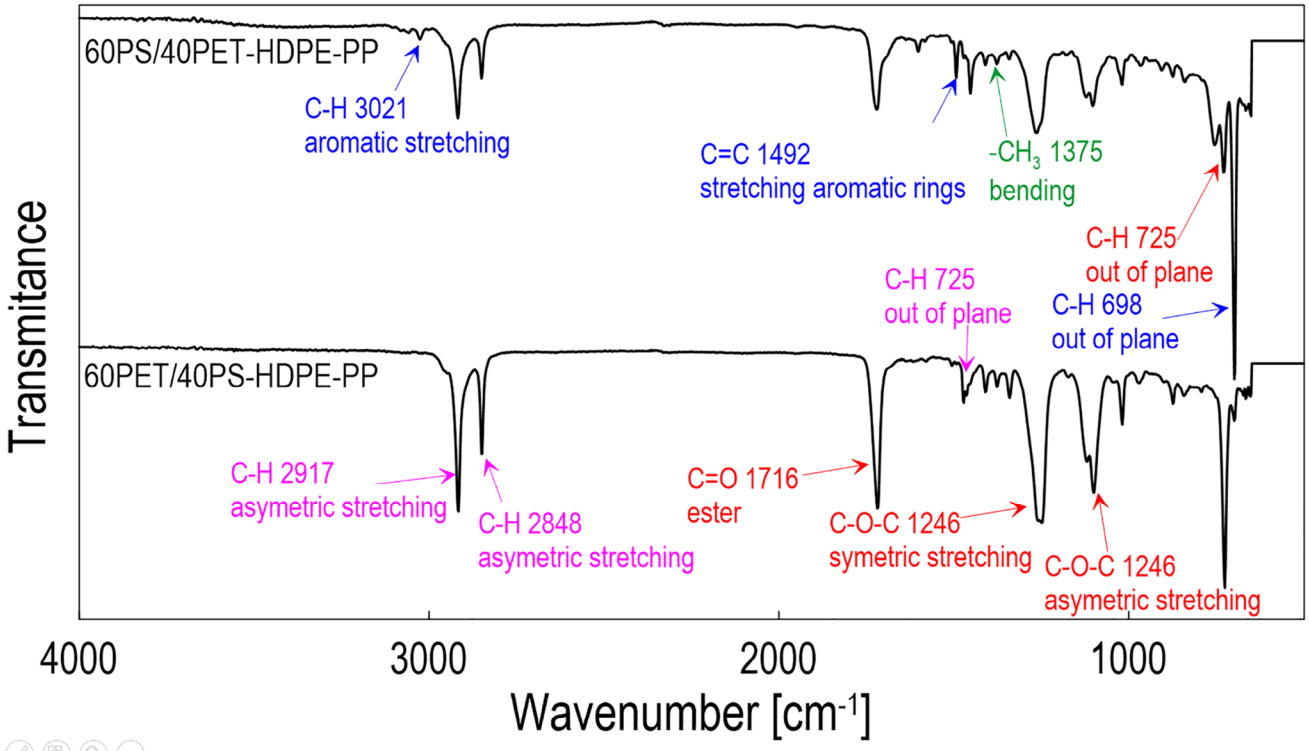

Figure 6. FTIR analysis (Nicolet iS 5 FTIR Spectrometer, Thermo Fisher Scientific, Waltham, MA, USA) of surfaces of waste compounds: PET (*red*), PS (*blue*), HDPE (*purple*), PP (*green*).

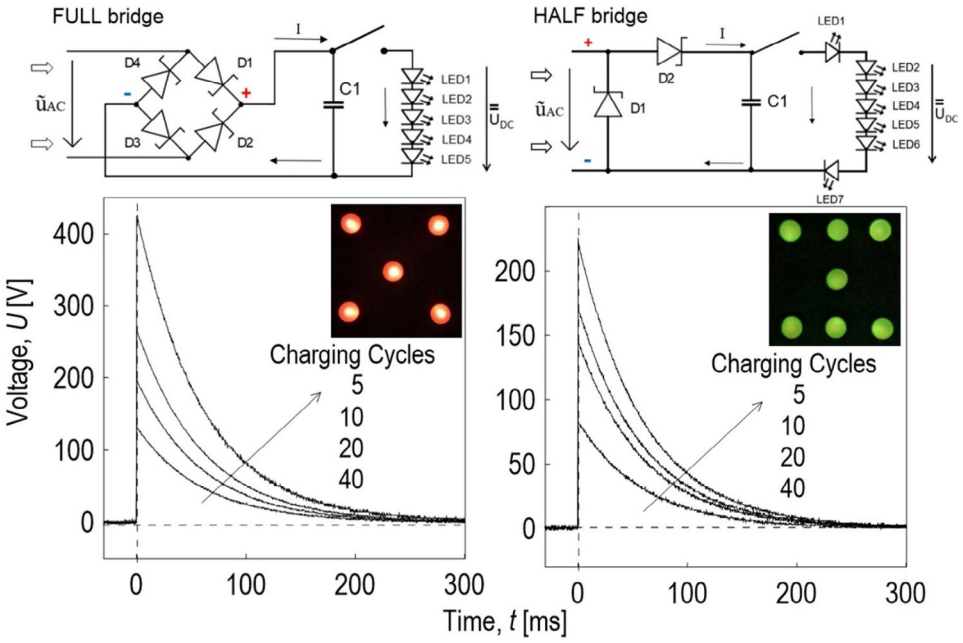

Figure 7. Schematics of full-bridge (upper) and half-bridge (lower) rectifiers based on Schottky diodes with a storage capacitor and LEDs, and time dependency of the discharge for different numbers of electrification cycles for triboelectric pair of PVDF and 60PET/40PS-HDPE-PP.

The setup of the triboelectric sensor based on PVDF and immiscible thermoplastic waste is shown schematically in **Figure 10**. In this way, the mutual movement of the dielectric and the electrode relative to each other and possible electrification at the electrode-polymer interface is prevented. Here, the PVDF and 60PET/40HDPE-PS-PP films are already in contact with a pressure force of 0.2 kPa imposed by the steel plate. Thus, the derived initial pressure force makes the sensor arrangement more compact. When a pressure pulse is applied from a macroscopic perspective, there is no mutual displacement of the individual dielectric layers relative to each other. However as shown by the surface topography and the cross-sectional profiles of polymeric films in Figure 1, the materials do not have the possibility to contact each other perfectly due to their roughness. When a pressure pulse is applied, the individual parts of the layers can continue to move relative to each other, the surfaces acquire a different, more perfect form of contact, which is the principle of the expected triboelectricity.

This arrangement also led to significantly higher output voltage values than when separate polymer layers were used. This triboelectrification resulted in reaching the value of an output voltage of 40 V for the conditions of the experiment. In conclusion, it should be noted that it was measured that, logically, the speed of

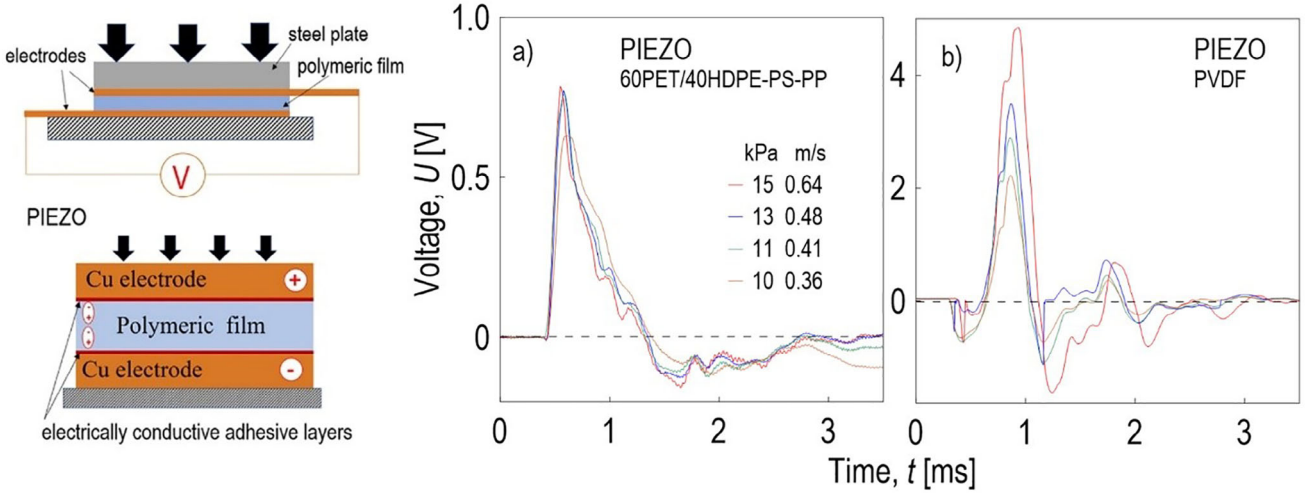

Figure 8. Schematic arrangement of the piezoelectric self-powered pressure stimulus sensor and the resulting output voltages for (a) 60PET/40HDPE-PS-PP polymeric film and (b) PVDF membrane.

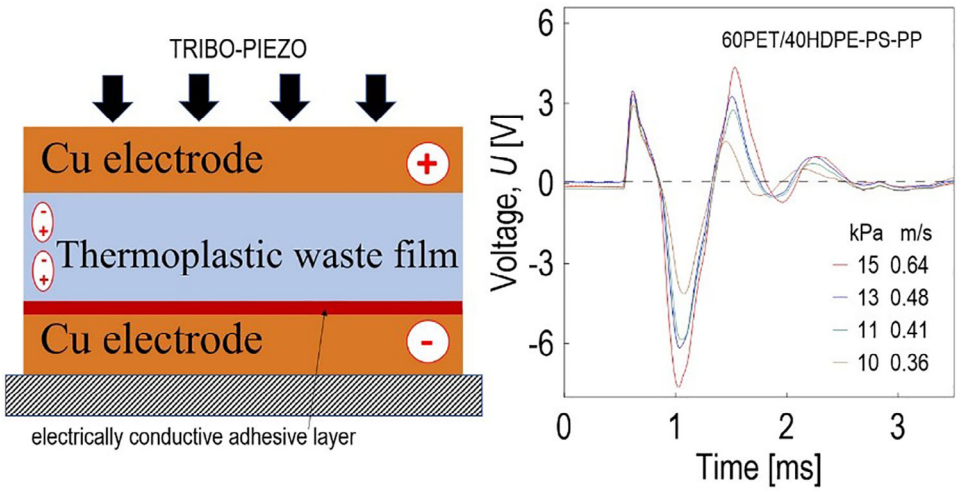

Figure 9. Schematic arrangement of the combined tribo-piezoelectric self-powered pressure stimulus sensor and the resulting output voltages of 60PET/40HDPE-PS-PP polymeric film.

the impact and the maximum stress during the impact increased this response.

4. Conclusion

Utilizing thermoplastic waste paired with PVDF can significantly reduce the production costs and environmental impacts of PVDF-based harvesters and sensors. In this study, an output voltage of nearly 800 V was obtained for a PVDF mat combined with a waste compound containing 60 wt. % of PET - poly(ethylene terephthalate) coming from a soft drink bottle and 40 wt.% of evenly distributed commodity waste originally used as dishwashing liquid bottle (HDPE – high-density polyethylene), meat packaging tray (PP – polypropylene), and cheese tray (PS – polystyrene). A nanogenerator made of such tribological pairs aligns well with global sustainability, where the reduction of plastic waste is a pressing issue.

The design of the sensors was examined in terms of the possible movements of the triboelectric pairs, as well as the movement of the individual tested films to the electrodes, aiming to distinguish the piezoelectric and triboelectric contributions.

The combination of the high piezoelectricity, mechanical performance, and chemical stability of polyvinylidene fluoride with easy-to-process, flexible, and environmentally benign recycled plastics enables a wide range of innovative applications such as wearable textiles, biomedical devices, and self-powered electronics with considerable output voltage values up to 800 V. This innovative strategy contributes to the circular economy and development of efficient energy harvesting technologies.

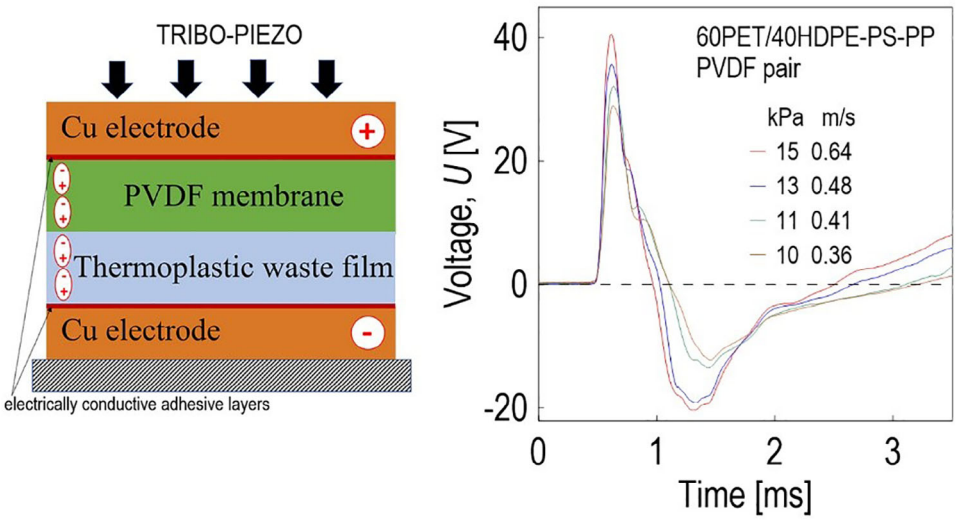

Figure 10. Schematic arrangement of the combined tribo-piezoelectric self-powered pressure stimulus sensor and the resulting output voltages PVDF membrane and 60PET/40HDPE-PS-PP polymeric film.

Acknowledgements

The authors acknowledge the Ministry of Education, Youth, and Sports of the Czech Republic, DKRVO (RP/CPS/2024-28/005).

Conflict of Interest

The authors declare no conflict of interest.

Author Contributions

Conceptualization was done by P.S. and B.H.; the methodology was developed by P.S., R.O., and J.M.; validation was performed by P.S.; formal analysis was conducted by P.S.; the investigation was carried out by P.S.; resources were provided by P.R. and B.H.; data curation was handled by P.S., R.O., and V.P.; the original draft was prepared by B.H. and P.R.; writing—review and editing was done by B.H.; visualization was managed by P.S. and B.H.; and funding acquisition was secured by B.H. and P.S. All authors read and agreed to the published version of the manuscript.

Data Availability Statement

The data that support the findings of this study are available from the corresponding author upon reasonable request.

Keywords

immiscible thermoplastic waste, nanogenerators, piezoelectricity, polyvinylidene fluoride, triboelectricity

Received: January 23, 2025
Revised: March 28, 2025
Published online:

[1] K. R. Kaja, S. Hajra, S. Panda, M. A. Belal, U. Pharino, H. Khanbareh, N. Vittayakorn, V. Vivekananthan, C. Bowen, H. J. Kim, *Nano Energy* **2024**, *131*, 110319.
[2] J. Kujawa, S. Boncel, S. Al-Gharabli, S. Koter, A. Kaczmarek-dziera, E. Korczeniewski, A. P Terzyk, *Chem. Eng. J.* **2024**, *492*, 151856.
[3] M. Koç, Ç. E. D. Dönmez, L. Paralı, A. Sarı, S. Aktürk, *J. Mater. Sci.: Mater. Electron.* **2022**, *33*, 8048.
[4] S. Panda, S. Hajra, K. Mistewicz, P. In-na, M. Sahu, P. M. Rajaitha, H. J. Kim, *Nano Energy* **2022**, *100*, 107514.
[5] V. S. Niranjana, J. U. Yoon, I. Woo, P. Gajula, J. W. Bae, A. A. Prabu, *Adv. Sustainable Syst.* **2024**, *8*.
[6] H. M. Venkatesan, S. R. Mohammad, S. Ponnan, K. J. Kim, P. Gajula, H. Kim, A. P. Arun, *Nano Energy* **2024**, *129*, 110003.
[7] X. Tao, H. Jin, M. Ma, L. Quan, J. Chen, S. Dong, H. Zhang, C. Lv, Y. Fu, J. Luo, *Phys. Status Solidi A* **2019**, *216*, 1900068.
[8] P. Slobodian, R. Olejnik, J. Matyas, P. Riha, B. Hausnerova, *Nano Energy* **2023**, *118*, 108986.
[9] J. P. Lange, *ACS Sustainable Chem. Eng.* **2021**, *9*, 15722.
[10] Y. Pang, Y. Cao, M. Derakhshani, Y. Fang, Z. L. Wang, C. Cao, *Matter* **2021**, *4*, 116.
[11] J. Zhang, Y. He, C. Boyer, K. Kalantar-Zadeh, S. Peng, D. Chu, C. H. Wang, *Nanoscale Adv.* **2021**, *3*, 5465.
[12] J. Z. Minhas, M. A. M. Hasan, Y. Yang, *Nanoenergy Adv.* **2021**, *1*, 131.
[13] A. Šutka, A. Šutka, H. Dundurs, B. del Rosal, M. Iesalnieks, K. Mālnieks, A. Linarts, A. J. Barlow, R. T. Leon, A. V. Ellis, P. C. Sherrell, *Adv. Energy Sustainability Res.* **2024**, *5*, 2300259.
[14] M. U. Bukhari, A. Khan, K. Q. Maqbool, A. Arshad, K. Riaz, A. Bermak, *Energy Rep.* **2022**, *8*, 1687.
[15] X. Feng, Q. Li, K. Wang, *ACS Appied Mater. Interf.* **2021**, *13*, 400.
[16] M. Navaneeth, S. Potu, A. Babu, B. Lakshakoti, R. K. Rajaboina, K. K. Uday, H. Divi, P. Kodali, K. Balaji, *ACS Sustainable Chem. Eng.* **2023**, *11*, 12145.
[17] H. Varghese, A. Chandran, *ACS Appl. Mater. Interfaces* **2021**, *13*, 51132.
[18] M. Navaneeth, P. Supraja, A. Babu, K. U. Kumar, K. Prakash, R. R. Kumar, *Mater. Lett.* **2023**, *336*, 133866.
[19] M. Sahu, S. Hajra, H. G. Kim, H. G. Rubahn, Y. Kumar Mishra, H. J. Kim, *Nano Energy* **2021**, *88*, 106255.
[20] G. Khandelwal, A. Chandrasekhar, N. R. Alluri, V. Vivekananthan, N. P. M. J. Raj, S. Kim, *Appl. Energy* **2018**, *219*, 338.
[21] M. Navaneeth, S. Potu, A. Babu, R. K. Rajaboina, U. K. Kumar, H. Divi, P. Kodali, K. Balaji, *Environmental Science: Adv.* **2023**, *6*, 848.
[22] E. N. Kalali, S. Lotfian, M. E. Shabestari, S. Khayatzadeh, C. Zhao, H. Y. Nezhad, *Current Opin. Green Sustainab. Chem.* **2023**, *40*, 100763.
[23] P. Slobodian, R. Olejnik, J. Matyas, B. Hausnerova, P. Riha, R. Danova, D. Kimmer, *Int. J. Mol. Sci.* **2022**, *23*, 14322.
[24] S. Ye, C. Cheng, X. Chen, X. Chen, J. Shao, J. Zhang, H. Hu, H. Tian, X. Li, L. Ma, W. Jia, *Nano Energy* **2019**, *60*, 701.
[25] D. Zhang, X. Zhang, X. Li, H. Wang, X. Sang, G. Zhu, Y. Yeung, *Eur. Polym. J.* **2022**, *166*, 110956.
[26] S. Panda, S. Hajra, H. Jeong, B. K. Panigrahi, P. Pakawanit, D. Dubal, S. Hong, H. J. Kim, *Nano Energy* **2022**, *102*, 107682.
[27] V. Singh, B. Singh, *J. Alloys Compd.* **2023**, *941*, 168850.
[28] B. S. Athira, A. George, K. Vaishna Priya, U. S. Hareesh, E. B. Gowd, K. P. Surendran, A. Chandran, *ACS Appl. Mater. Interfaces* **2022**, *14*, 44239.
[29] H. Chen, L. Zhou, Z. Fang, S. Wang, T. Yang, L. Zhu, X. Hou, H. Wang, Z. L. Wang, *Adv. Funct. Mater.* **2021**, *31*, 2011073.
[30] C. Luo, Y. Shao, H. Yu, H. Z. Ma, Y. H. Zhang, L. Gu, B. Yin, M. B. Yang, *Chem. Phys. Lett.* **2023**, *813*, 140276.
[31] S. S. Rana, M. T. Rahman, M. Salauddin, S. Sharma, P. Maharjan, T. Bhatta, H. Cho, C. Park, J. Y. Park, *ACS Appl. Mater. Interfaces* **2021**, *13*, 4955.
[32] A. Babu, K. Ruthvik, P. Supraja, M. Navaneeth, K. U. Kumar, R. R. Kumar, K. Prakash, N. Raju, *J. Mater. Sci.: Mater. Electron.* **2023**, *34*, 2195.
[33] T. Bhatta, S. Sharma, K. Shrestha, Y. Shin, S. Seonu, S. Lee, D. Kim, M. Sharifuzzaman, S. M. Rana, J. Y. Park, *Adv. Funct. Mater.* **2022**, *32*, 2202145.
[34] Y. J. Kim, J. Lee, S. Park, C. Park, C. Park, H. J. Choi, *RSC Adv.* **2017**, *7*, 49368.
[35] G. Min, L. Manjakkal, D. M. Mulvihill, R. S. Dahiya, *IEEE Sens. J.* **2020**, *20*, 6856.
[36] X. Kang, C. Pan, Y. Chen, X. Pu, *RSC Adv.* **2020**, *10*, 17752.
[37] M. P. Kim, D. S. Um, Y. E. Shin, H. Ko, *Nanoscale Res. Lett.* **2021**, *16*, 35.
[38] A. Ghaffarinejad, J. Y. Hasani, D. Galayko, P. Basset, *Nano Energy* **2019**, *66*, 104137.
[39] R. Stepancikova, R. Olejnik, J. Matyas, M. Masar, B. Hausnerova, P. Slobodian, *Sensors* **2024**, *24*, 1275.